Io-related Jovian auroral arcs: Modeling parallel electric fields

Yi-Jiun Su, Robert E. Ergun, Fran Bagenal, and Peter A. Delamere
Laboratory for Atmospheric and Space Physics, University of Colorado, Boulder, Colorado, USA

Received 4 January 2002; revised 13 November 2002; accepted 30 December 2002; published 28 February 2003.

[1] Recent observations of auroral arcs on Jupiter suggest that electrons are being accelerated downstream from Io's magnetic footprint, creating detectable emissions. The downstream electron acceleration is investigated using one-dimensional spatial, two-dimensional velocity static Vlasov solutions under the constraint of quasi-neutrality and an applied potential drop. The code determines self-consistent charged particle distributions and potential structure along a magnetic field flux tube in the upward (with respect to Jupiter) current region of Io's wake. The boundaries of the flux tube are the Io torus on one end and Jupiter's ionosphere on the other. The results indicate that localized electric potential drops tend to form at 1.5–2.5 R_J Jovicentric distance. A sufficiently high secondary electron density causes an auroral cavity to be produced similar to that on Earth. Interestingly, the model results suggest that the proton and the hot electron population in the Io torus control the electron current densities between the Io torus and Jupiter and thus may control the energy flux and the brightness of the aurora downstream from Io's magnetic footprint. The parallel electric fields also are expected to create an unstable horseshoe electron distribution inside the auroral cavity, which may lead to the shell electron cyclotron maser instability. Results from our model suggest that in spite of the differing boundary conditions and the large centrifugal potentials at Jupiter, the auroral cavity formation may be similar to that of the Earth and that parallel electric fields may be the source mechanism of Io-controlled decametric radio emissions. *INDEX TERMS:* 2708 Magnetospheric Physics: Current systems (2409); 2756 Magnetospheric Physics: Planetary magnetospheres (5443, 5737, 6030); 2736 Magnetospheric Physics: Magnetosphere/ionosphere interactions; 2704 Magnetospheric Physics: Auroral phenomena (2407); *KEYWORDS:* Jupiter-Io interaction, Io wake emission, electron precipitation, upward current region, auroral cavity, decametric radio emission

Citation: Su, Y.-J., R. E. Ergun, F. Bagenal, and P. A. Delamere, Io-related Jovian auroral arcs: Modeling parallel electric fields, *J. Geophys. Res.*, *108*(A2), 1094, doi:10.1029/2002JA009247, 2003.

1. Introduction

[2] The electromagnetic interaction between Jupiter and Io has been studied extensively since the 1964 discovery of Io-controlled decametric radio emission (DAM) [*Bigg*, 1964]. These emissions, largely thought to be from the electron cyclotron maser instability, as is on Earth [*Le Quéau et al.*, 1983; *Zarka*, 1998], suggest that Io induces an electromagnetic disturbance on Jupiter's magnetic flux tubes. A variety of mechanisms for the electromagnetic disturbance have been examined, including a unipolar induction electric field across Io producing a current loop closing in Jupiter's ionosphere [*Goldreich and Lynden-Bell*, 1969], the excitation of large-amplitude Alfvén waves [*Neubauer*, 1980], and the generation of electrostatic electric fields parallel to ambient magnetic field [*Crary*, 1997]. The latter mechanisms have been advanced on the basis of Voyager and Galileo observations.

[3] Jovian auroras have been imaged in the ultraviolet, X ray, and infrared wavelengths. In addition to the main and secondary auroral ovals, these images reveal low-latitude auroral "spots" at the footprints of Jovian satellites, the brightest of these being associated with Io [*Clarke et al.*, 1996, 2002; *Prangé et al.*, 1996]. In addition to the spots, an extended tail of emissions downstream of Io's magnetic footprint has been resolved [*Clarke et al.*, 1996]. These recent images have motivated *Delamere et al.* [2003] to divide the Io-Jupiter interaction into three phases: (1) initial mass loading interaction, (2) acceleration of plasma in the wake of Io, and (3) steady state decoupling. *Delamere et al.* [2003] suggest that the first two phases may induce an Alfvénic disturbance that is related to the bright emissions at Io's magnetic footprint, whereas the third phase sets up field-aligned currents in the downstream region of Io's wake. In this paper we focus on the static parallel electric fields in the upward (with respect to Jupiter) current region of Io's wake (i.e., phase 3 interaction) and do not address the disturbance at Io's magnetic footprint.

[4] Figure 1 displays a Jovian auroral image taken by the NASA Hubble Space Telescope (HST) [after *Clarke et al.*, 2002, Figure 1b]. The Io-induced aurora is seen at the left, with the brightest emissions at the base of the Io flux tube and a faint emission tail extending eastward. By analyzing

0148-0227/03/2002JA009247$09.00

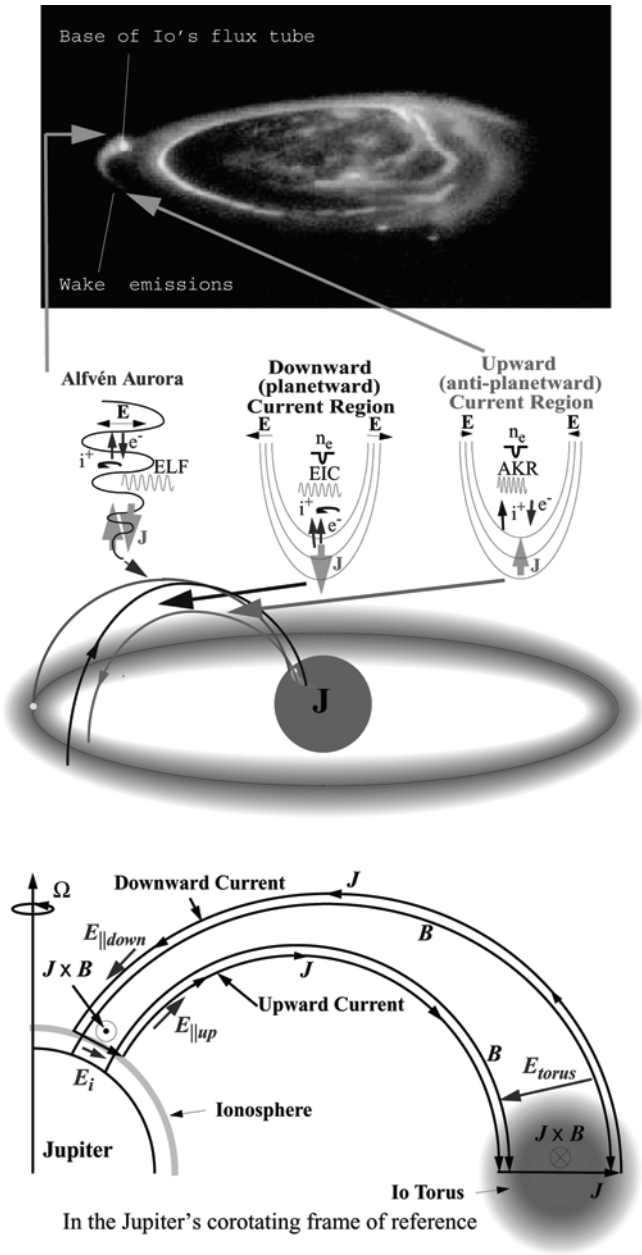

Figure 1. The top panel shows a Jovian auroral image taken by the Hubble Space Telescope [after *Clarke et al.*, 2002, Figure 1b], where the Io-induced aurora is seen on the left with the brightest emissions at the base of the Io flux tube and an emission trail extending downstream. A depiction of the three types of Jovian auroral regions is shown in the middle panel, where the green, blue, and red lines represent the Alfvén-dominated region, the downward current region, and the upward current region, respectively. The quasi-static current structure downstream of Io's wake in the Jupiter's corotating frame of reference is illustrated in the bottom panel, where black and blue lines are used to represent the magnetic field and electric current, respectively. Green arrows are used to show the electric field, where $E_{\text{torus}} = E_i + E_{\|\text{up}} + E_{\|\text{down}}$. See color version of this figure at back of this issue.

HST Goddard High Resolution Spectrograph (GHRS) auroral spectra of the 1200–1700 Å region, *Dols et al.* [2000] suggested that the electron population responsible for the excitation of the Io footprint has a mean energy of about 60 keV. This approximation is comparable to the result of a model in which electron fluxes are accelerated to 75 keV by repeated Fermi acceleration in parallel electric fields generated by Alfvén waves [*Crary*, 1997]. One of the theoretical frameworks suggested by *Clarke et al.* [2002] is that an induction electric field across the plasma stripped from Io could produce a current loop which closes in Jupiter's ionosphere, similar to the interaction at Io itself but with a lower amplitude. *Hill and Vasyliunas* [2002] used four cases of observed tail emissions from *Clarke et al.* [2002] to show the reduction in brightness with distance to be approximately exponential with an *e*-folding length of $\sim 12^\circ$ of longitude. On the basis of Space Telescope Imaging Spectrograph (STIS) spectral observations of the Io footprint and tail and using electron precipitation and Jovian atmosphere models, *Gérard et al.* [2002] suggest that the electron mean energies drop from typical 70 keV on the footprint to 30 keV 20° downstream of the Io footprint. The decrease in brightness along the tail is consistent with a decrease of the electron energy flux due to a decrease of characteristic energy and a decrease of the number flux of precipitating electrons.

[5] Recently, *Mauk et al.* [2002] indicated several similarities between the Earth's aurora and Io's auroral emissions and tail. *Ergun et al.* [2002b] support this idea by suggesting the three types of auroral acceleration regions observed by the Fast Auroral SnapShoT (FAST) to be active magnetosphere-ionosphere (MI) coupling processes on Jupiter. The three regions can be classified as an Alfvénic acceleration region, a downward (with respect to the planet) current region, and an upward current region. An illustration depicting the three types of auroral regions is displayed directly below the HST auroral image in Figure 1. The quasi-static current structure downstream of Io's wake is illustrated in the bottom of Figure 1 (see the figure caption for a more detailed description).

[6] In the Earth's magnetosphere the Alfvénic acceleration region is near the open-closed field line boundary where particle acceleration is dominated by Alfvénic fluctuations. The most intense counterstreaming electron fluxes are driven by propagating Alfvén waves associated with oscillating parallel electric fields [*Chaston et al.*, 1999; *Lotko et al.*, 1998; *Lysak*, 1998]. *Crary* [1997] and *Ergun et al.* [2002b] suggest that the bright emissions at the Io magnetic footprint are caused by Alfvén-dominated precipitation.

[7] The strongest indications of an active downward current region in the Jupiter-Io system are field-aligned or bidirectional energetic electron fluxes that have been observed near Io [*Frank and Paterson*, 1999a, 2000]. *Mauk et al.* [2001] intimated that the Io electron beams are created at low Jovian altitudes in a downward current region. They drew their conclusions by comparing electron distributions with bidirectional electron fluxes in the Earth's central plasma sheet with those near Io. FAST satellite observations have demonstrated that antiearthward (antiplanetward) field-aligned electron beams accelerated by parallel electric fields are a feature of the downward current region [*Carlson*

et al., 1998; *Ergun et al.*, 1998]. *Andersson et al.* [2002] reported a direct measurement of the parallel electric field in the downward current region, strongly supporting the earlier results. The downward current region is not as steady as the upward current region, is often combined with the Alfvénic fluctuations, and rarely is associated with detectable auroral emissions.

[8] The upward current region is the well-established and long-studied acceleration region in the Earth's aurora. Parallel electric fields are known to be the primary acceleration mechanism of the upward current region. Direct measurements of parallel electric fields have been reported by *Mozer and Kletzing* [1998] and *Ergun et al.* [2001a, 2002a] from the Earth's polar orbiting satellites. The prominent features of the upward current region are the downgoing (planetward) accelerated electrons and up-going (antiplanetward) accelerated ions. This region is bound by strong converging electric fields that surround a low-density cavity which is known to be the source of auroral kilometric radiation (AKR). It was demonstrated by FAST observations [*Ergun et al.*, 2000b] that the AKR source mechanism is a "shell" electron cyclotron maser directly associated with charged particle acceleration from magnetic field-aligned electric fields. It is possible, then, that the Io-controlled DAM is an indicator of electron acceleration by parallel electric fields.

[9] In this paper we explore the possibility that the extended tail emissions in Io's wake are due to electron acceleration from parallel electric fields in an upward current region between Jupiter and Io. We will not address the observation of Io electron beams, possibly from a downward current region, or the Alfvén wave phenomena that are possibly active at the Io footprint. Here we adopt the framework of a static kinetic Vlasov code [*Ergun et al.*, 2000a] that was used to model the Earth's upward current region. The model is modified to include conditions that apply to Jupiter's upward current region of Io's wake (see section 2). The solutions with various boundary conditions are presented in section 3.

2. Model Description

[10] In this paper a static, one-dimensional spatial, two-dimensional velocity, kinetic Vlasov code is used to search for large-scale, self-consistent solutions of parallel electric fields at Io's wake. A magnetic flux tube was adopted at $L = 5.9$ from Jupiter's ionosphere to the center of Io torus at the equatorial plane (shown in the top panel of Figure 2). The net potential drop between Jupiter and Io is specified.

[11] The spatial domain (distance along the flux tube) is divided evenly into N_s (= 51) grids along a dipole magnetic field line. The Vlasov code includes the magnetic mirror effect, as well as the gravitational and centrifugal potentials. The gravitational and centrifugal potentials based on the O^+ species are displayed in the bottom panel of Figure 2, where the dotted and dashed lines represent the gravitational potential and the centrifugal potential, respectively, while the solid line represents a combination of gravitational and centrifugal potentials. The horizontal axis represents Jovicentric distance in Jupiter radii (R_J). The left- and right-hand sides are the ionospheric and Io boundaries, respectively.

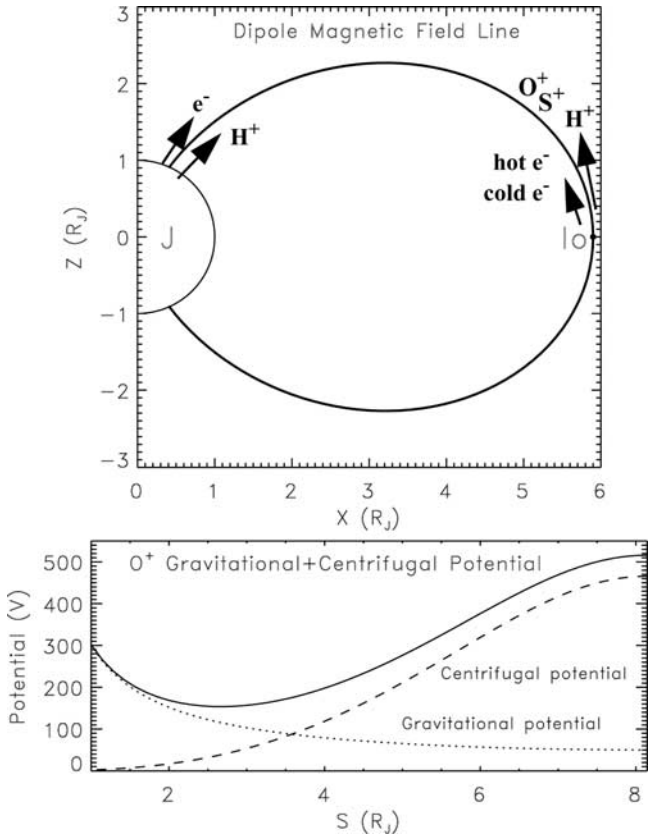

Figure 2. (top) Dipole magnetic flux tube at $L = 5.9$. (bottom) Gravitational and centrifugal potentials along the magnetic field line on the basis of O^+ species.

The minimum potential is located at ~2.5 R_J along the flux tube.

[12] Cold ionospheric electrons and ions are prescribed as fluids at Jupiter's ionospheric boundary, while Io-generated plasma species are assigned as Maxwellian distributions at the Io boundary. In some cases, secondary (backscattered) electrons are included as a kappa distribution function (κ = 4, L. Andersson, personal communication based on the FAST observations, 2002). The distribution functions are broken into $N_v \times N_v$ velocity-space elements ($N_v = 50$), each of which is treated as a fluid. The potentials at both upper and lower boundaries must be fixed throughout the simulation. An estimated electric potential profile, $\Phi(s)$, is initiated in the model. Using the prescribed parameters at the boundaries and $\Phi(s)$, the velocity-space distributions are then calculated along the magnetic field line.

[13] The basic idea is to solve the Poisson's equation along the field line. An error is defined as

$$\xi(s) = \nabla^2\Phi(s) + e[n_i(s) - n_e(s)]$$

where $n_i(s)$ and $n_e(s)$ are the ion and electron densities calculated from the distribution functions. We iteratively adjust the electric potential $\Phi(s)$ to minimize the error $\xi(s)$, which yields a steady state solution. The spatial grid size of the model is much larger than the Debye length ($\lambda_D < 1$ km); hence the first term on the right-hand side of the equation is negligible, essentially resulting in a quasi-

neutral solution. The quasi-static model enforces adiabatic evolution without velocity-space diffusion.

[14] The Vlasov code was validated by the linear Knight relation [*Knight*, 1973; *Lyons*, 1980]:

$$j = K\Phi, K = \frac{e^2 n}{\sqrt{2\pi m_e T_e}},$$

where j and Φ are parallel current density and parallel potential. T_e, m_e, n, and e are electron temperature, mass, density, and charge. The Knight relation is only linear in a range of $1 \ll e\Phi_{\|}/k_B T_e \ll R_M$, where R_M is mirror ratio ($\sim$400 for the Io flux tube). It should be noted that current densities calculated from the particles (primary electrons) of Vlasov solutions in our paper are not identical to those calculated by the Knight relation simply because the linear requirement does not apply.

3. Vlasov Solutions

3.1. Boundary Conditions

[15] The solution of the static Vlasov code is driven by the boundary conditions. The plasma conditions in flux tubes of the extended wake downstream of Io are not known. A dense, cold plasma was measured by Galileo 1.4 R_J downstream, but how this plasma evolves and mixes with the background torus plasma while traveling $\sim$100° (in $\sim$3 hours) around Jupiter is unknown. For this initial study we take plasma conditions typical of the background torus but note that our ignorance of the true conditions, particularly at high latitudes, is a serious limitation of studies of the wake aurora.

[16] Cold electrons and protons are introduced at Jupiter's ionospheric boundary [*Dessler*, 1983, chapter 2], while O^+, S^+, and electrons are assigned at the Io boundary. The ion composition and temperature in the Io plasma torus are based on results published by *Bagenal* [1994] and *Crary et al.* [1998], with the simplification of omitting S^{++} and the minor species of O^{++} and S^{+++}. Oxygen ions are chosen to represent both mass/charge = 16 ion species (O^+ and S^{++}). The average temperatures of O^+ and S^+ are assumed to be 50 eV. In this paper, O^+ ions are assigned the temperature anisotropy of 2 (i.e., $T_{\|}$ = 35 and $T_{\perp}$ = 70). The number of heavy ion species have been limited in the model to minimize computer processing time.

[17] In addition to the plasma boundary conditions, the boundary condition of the electric potential is an important parameter in determining the precipitating electron energy and energy flux. Auroral emissions are a result of the high-energy precipitating electrons. On the basis of ultraviolet emissions observed by HST, *Clarke et al.* [2002] reported that the brightness is of the order of tens of kilorayleigh (kR) 20° downstream of Io's footprint (see their Figure 3). Previous studies [*Gérard et al.*, 2002; *Grodent et al.*, 2001; *Waite et al.*, 1983; *Gérard and Singh*, 1982] indicated that the efficiency of the electron energy conversion is close to 10 kR erg^{-1} cm^{-2} s^{-1} for primary energies between 10 and 100 keV. On the basis of suggestions from *Gérard et al.* [2002] that the mean energy of electrons 20° downstream of Io's footprint is $\sim$30 keV, a negative 30 kV potential is selected and fixed at the Io boundary in all cases presented in this paper. Assuming a potential of tens of kV (i.e., tens of keV precipitating electron energy), a current density of the order of 0.1 μA m^{-2} is required to obtain a converted energy flux of the order of 1 erg cm^{-2} s^{-1}. The current density referred to throughout the paper is converted to its corresponding value at the base of the flux tube. Because of limitations of the instrument resolution, the estimated current density may be representative of a lower limit. The fine structures of auroral arcs may be a result of the higher current density and energy flux in the flux tube (see discussion).

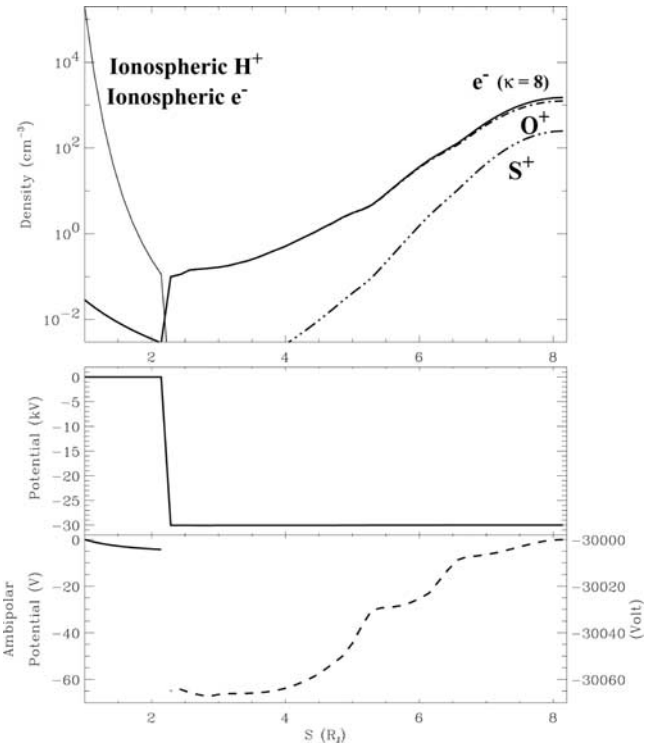

Figure 3. (top) Density profiles for five species shown in Table 1. The ionospheric protons and electrons are represented by the thin solid and dotted lines. The bold solid, dash-dotted, triple dash-dotted lines represent the e^-, O^+, and S^+, respectively, at the Io boundary. (middle) Electric potential profile. (bottom) The solid line represents the potential below 2.2 R_J, while the dashed line represents the potential above 2.2 R_J.

3.2. Baseline Solution

[18] In case 1, a baseline solution is obtained for the current density (0.4 μA m^{-2}) of the same order as that calculated from observations [*Gérard et al.*, 2002]. A solution of case 1 is shown in Figure 3. The corresponding boundary conditions of case 1 are listed in Table 1. In the top panel of Figure 3, the bold solid, dash-dotted, and triple dash-dotted lines represent electron, O^+, and S^+ species of Io plasma, while the thin solid and dotted lines represent the ionospheric H^+ ions and electrons. The horizontal axis represents the Jovicentric distance along the flux tube from Jupiter to the torus. Io electrons are assumed to be a kappa distribution where κ = 8 is used to represent electrons with a slightly hotter tail than a Maxwellian distribution. Ionospheric electron and ion levels below the potential jump are

Table 1. Boundary Conditions of Case 1

Species	Density	Temperature	Boundary
Ionospheric H^+	2×10^5 cm^{-3}	0.31 eV	left
Ionospheric e^-	2×10^5 cm^{-3}	0.31 eV	left
Io O^+	1000 cm^{-3}	$T_\parallel = 35$; $T_\perp = 70$	right
Io S^+	250 cm^{-3}	50 eV	right
Io e^-	1250 cm^{-3}	4.9 eV[a]	right

[a]In this case we assume the electrons as a kappa distribution ($\kappa = 8$) to present a cold population and a slightly hot tail.

identical, resulting in overlapping of the dotted and solid lines. An overlapping of the bold solid (Io electron) and dash-dotted (O^+) lines is also seen at $\sim$2–5 R_J.

[19] The electric potential profile along the flux tube is shown in the middle panel of Figure 3. A sharp potential jump occurs at $\sim$2.2 R_J, where the density of ionospheric species is comparable to that of the Io species. The width of this potential drop is much narrower than the resolution of the grid size, resulting in a sharp discontinuity. Below and above the large potential jump, ambipolar electric fields (of the order of few to tens of volts) are set up to maintain the quasi-neutrality. The ambipolar electric fields are shown in the bottom panel of Figure 3, where the solid and dashed lines represent the potential below and above the potential jump, respectively.

[20] It should be noted that Vlasov solutions may not be unique. For example, a family of self-consistent solutions can be found within two spatial grids of the potential drop shown in Figure 3; however, we could find no solution where the potential drop would occur above 3.5 R_J. The quasi- neutral solutions indicate that the potential jump is a low-altitude phenomenon. The current density is found to decrease slightly if the potential jump is closer to the Jupiter and to increase slightly if the potential jump is farther away. However, the position of the potential is not as sensitive as other parameters, such as the anisotropic temperature of O^+ (see the next paragraph); the hot electron tail (discussed in section 3.3); and the concentration of H^+ in the Io plasma torus (discussed in section 3.5).

[21] In the solution shown in Figure 3, S^+ ions are confined by the centrifugal potential, resulting a density drop at $\sim$4 R_J. The lower A/Z ions (S^{++} and O^+, here represented by O^+) are less tightly confined to the equator. The O^+ ion distribution was assumed to have a temperature anisotropy ($T_\perp/T_\parallel$) of 2. The solution with an O^+ isotropic temperature of 50 eV was also examined (not shown here). The result indicates that the ion density is raised an order of magnitude higher in the region before the potential drop than that shown in Figure 3. This enhancement assists Io electrons to reach a higher density and carry an order of magnitude higher current density. Therefore the observed temperature anisotropy of the O^+ ion distribution in the Io torus strongly confines the O^+ to the torus and thus acts to reduce the electron energy flux to Jupiter.

3.3. Io Hot Electrons

[22] The effect of hot electrons is explored in Figure 4, which plots electron densities for three cases. The results of case 1 (also in Figure 3) show that the Io electrons with a kappa distribution ($\kappa = 8$) carry the current density of 0.4 μA m^{-2}. In case 2, a different Io electron distribution is chosen, with a kappa distribution of $\kappa = 4$ (i.e., a hotter tail

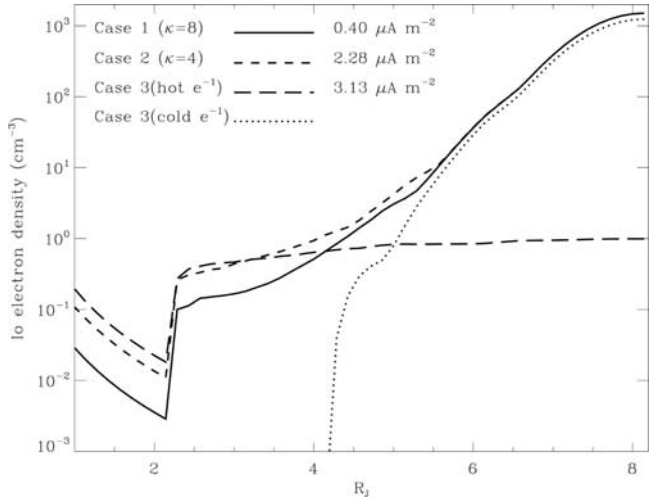

Figure 4. Io electron density profiles, where the solid line represents case 1 with $\kappa = 8$, the dashed line represents case 2 with $\kappa = 4$, and the long-dashed and dotted lines represent hot (200 eV) and cold (5eV) electrons of case 3.

in a kappa distribution). The remaining boundary conditions are the same as those in case 1. The resulting current density in case 2 (2.28 μA m^{-2}) is a clear indication that a hotter tail leads to a higher current density. In case 3, cold (5 eV) and hot (200 eV) Io electron Maxwellian distribution functions are chosen rather than a kappa function. The hot electron density is assumed to be as high as 0.1% of the total electron density at 5.9 R_J based on Voyager 1 observations reported by *Sittler and Strobel* [1987]. The resulting current density in case 3 (3.13 μA m^{-2}) is carried by hot electrons.

3.4. Secondary Electrons

[23] In cases 4 and 5 (Figure 5), secondary electrons [*Ajello et al.*, 2001] from Jupiter's auroral atmosphere are assigned as a kappa distribution function with $\kappa = 4$ (L. Andersson, personal communication based on the FAST

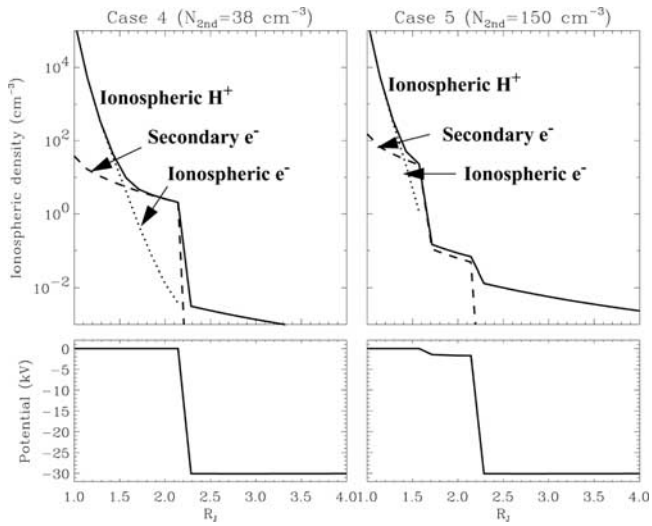

Figure 5. (top) Ionospheric plasma density profiles of case 4 (left) and case 5 (right). (bottom) Electric potential of case 4 (left) and case 5 (right).

Table 2. Boundary Conditions of Case 6

Species	Density	Temperature	Boundary
Ionospheric H^+	2×10^5 cm^{-3}	0.31 eV	left
Ionospheric e^-	2×10^5 cm^{-3}	0.31 eV	left
Secondary e^-	150 cm^{-3}	100 eV	left
Io O^+	1000 cm^{-3}	$T_\parallel = 35$; $T_\perp = 70$	right
Io S^+	250 cm^{-3}	50 eV	right
Io H^+	1 cm^{-3}	200 eV	right
Io cold e^-	1250 cm^{-3}	5 eV	right
Io hot e^-	1 cm^{-3}	200 eV	right

observations, 2002) at the ionospheric boundary. In case 4, the densities of the secondary electrons are assumed to be 38 cm^{-3} with a temperature of ~100 eV. All other boundary conditions remain the same as those used in case 3. The ionospheric plasma densities of the case 4 solution are plotted in the top left panel of Figure 5, where the solid, dotted, and dashed lines represent the cold proton density, the cold electron density, and the secondary electron density, respectively. The electric potential profile is shown in the bottom left panel, where a single potential jump was formed at ~2.2 R_J. Although the secondary electrons dominate the electron density above ~1.7 R_J, the potential distribution remains relatively unchanged from case 3.

[24] In case 5, the secondary electron density is increased to 150 cm^{-3} with all other boundary conditions remaining the same as those in cases 3 and 4. The solution from case 5, displayed on the right side of Figure 5, is dramatically different from the previous cases. With a high density of secondary electrons, the potential drop on the ionospheric side (at ~1.5 R_J of case 5) emerges in addition to the potential drop at 2.2 R_J. All possible solutions we could find under case 5 display the two potential drops as seen in the solutions at Earth [*Ergun et al.*, 2000a]. The underlying physics can be understood from the condition of quasi-neutrality. Under a high secondary electron density, the electron density exceeds the gravitationally bound ionospheric proton density at ~1.5 R_J. A strong parallel potential at low altitudes is required to satisfy the quasi-neutral condition. A stronger precipitating electron flux (and hence higher secondary electron density) causes the second potential drop to appear at a lower altitude.

3.5. Protons at Io Boundary

[25] The solution from case 1 suggests that heavy ions are tightly confined to the torus. On the other hand, light ions, such as protons, can spread along the flux tube due to the reduced centrifugal forces and can dominate the ion density at roughly 2–4 R_J. The presence of H^+ in the Io torus can dramatically affect the electron energy flux.

[26] While proton densities in the Jovian plasma sheet and cold inner torus are well determined by in situ measurements [*Dessler*, 1983, chapter 3], they are difficult to separate from high densities of heavy ions in the Io plasma torus. *Frank and Paterson* [1999b] reported a proton density of ~60 cm^{-3} measured by the PLS instrument on Galileo in the immediate vicinity of Io. They argued that half of these protons are local pickup protons, in which case they would be highly anisotropic ($T_\perp \gg T_\parallel$) and confined to the equator. *Chust et al.* [1999] inferred a lower limit for the H^+ density of 0.5% (10 cm^{-3} for total torus density of 2000) from Galileo plasma wave data near Io. Tighter constraints on the proton density at high latitudes (where protons dominate the composition) are provided by studies of wave propagation. Estimates of the proton density from modeling the dispersion of whistler waves (propagating from Jupiter to the torus) have steadily decreased from early estimates of 15–20% of the total flux tube content [*Tokar et al.*, 1982], to *Crary et al.*'s [1996] estimate of 5% (maximum density ~50 cm^{-3}), and, most recently, to the proton density of 3–8 cm^{-3} estimated by *Wang et al.* [1998a, 1998b] at high latitudes for torus L-shells. This constraint on proton density of ~5 cm^{-3} is consistent with limits placed on the total electron density at high latitudes from observed Faraday rotation of Jovian radio emission reported by *Melrose and Dulk* [1991]. Finally, we note that *Zarka et al.* [2001] estimated the proton concentration to be 1–3% of the torus density (20–60 cm^{-3}) in the Io wake region, based on the minimum frequency of Io-dependant decametric radio emission.

[27] In case 6, the Io H^+ density was assumed to be 1 cm^{-3} while a temperature of 50 eV (same energy as heavy ions) was assigned. All other boundary conditions remain the same as those in case 5. Boundary conditions for eight plasma species used in case 6 are listed in Table 2 and the solution is shown in Figure 6. The format of the top two panels is similar to that in Figure 3.

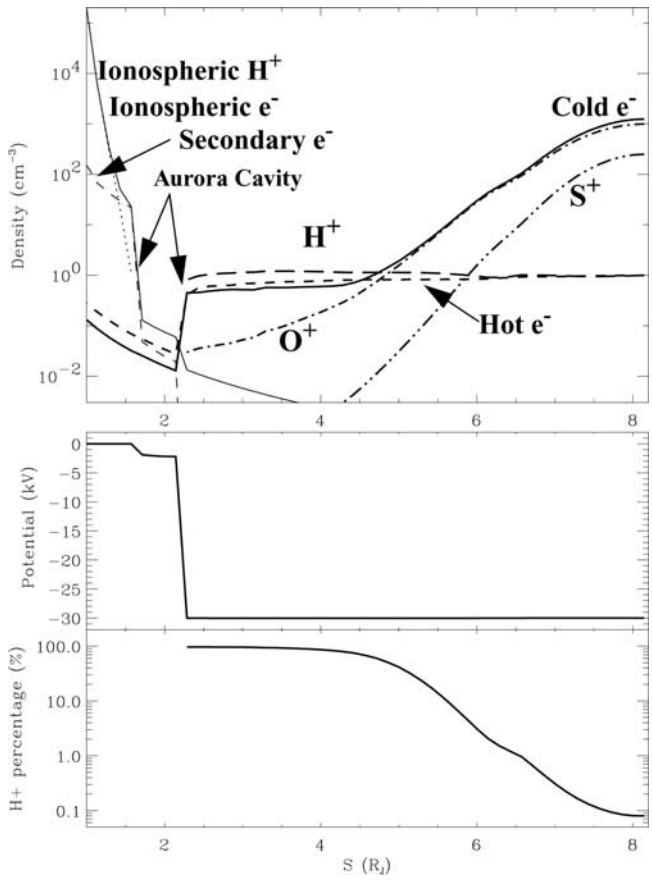

Figure 6. Solution of case 6. The format of the top two panels is the same as that in Figure 3 except that Io H^+ ions (bold long-dashed line), Io hot electrons (bold dashed line), and secondary electrons (dashed line) are included here. The percentage of Io H^+ ions along the field line is shown in the bottom panel.

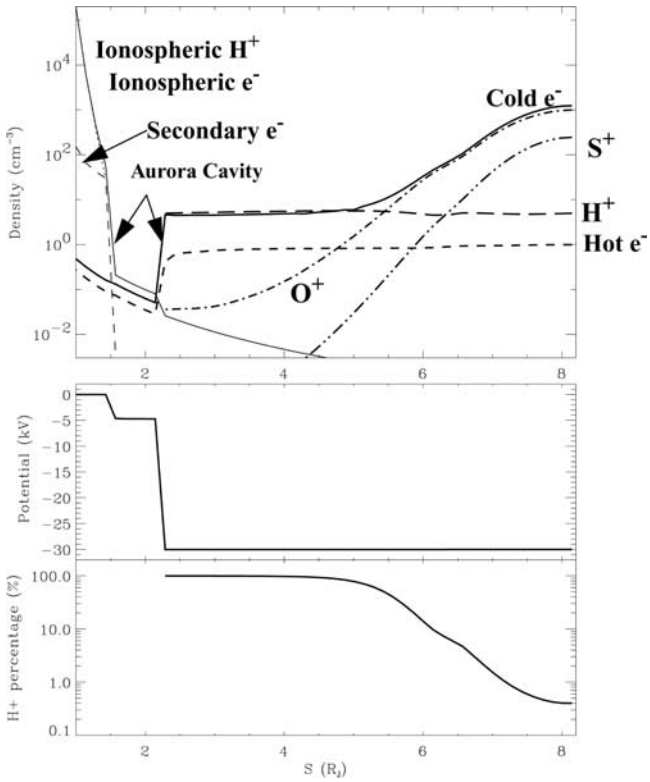

Figure 7. Solution of case 7. The figure format is the same as that in Figure 6 except that the Io H^+ ion density is assumed to be 5 cm^{-3} at the torus.

[28] In Figure 6 (case 6), Io H^+ ions become the dominant ion species directly above the potential drop at ~2.2 R_J; hence the heavy ions have a much smaller effect on generating the parallel electric field. The higher ion density at ~2 to ~4 R_J allows for more torus electrons to travel into that region and thus allows for a significant increase in electron energy flux. Essentially, the H^+ ions act as the base of a transistor, greatly amplifying the electron current even though the H^+ ions do not carry a significant current. In case 6, the current density is 6.94 μA m^{-2}, and two thirds of the current density is carried by hot electrons. The percentage of H^+ included within the total ion density is plotted in the bottom panel of Figure 6. The H^+ percentage increases away from the center of the plasma torus because major ion species are bound near the torus while H^+ ions are free to spread along the field line.

[29] The boundary condition of the Io H^+ density is increased to 5 cm^{-3} in case 7, while conditions for other plasma species remain the same. The solution from case 7 is displayed in Figure 7. At altitudes directly above the potential drop at ~2.2 R_J, the total electron density is about 6 times higher than that shown in the previous case. The current density is now raised to 32.54 μA m^{-2}, two orders of magnitude higher than the estimated value based on HST observations. The current density calculated by hot electrons is similar as that of case 6; however, the cold electrons become the primary current carrier. Some density fluctuations are seen in Figures 3, 4, 6, and 7 due to the decay of heavy ions and also near the transition regions of the different ion species; however, these small fluctuations do not affect our solutions.

Table 3. Current Densities at Jupiter's Ionosphere

Case	J_{total}	$J_{hot\ e-}$	$J_{cold\ e-}$
Case 1	0.40 μA/m^2	-	-
Case 2	2.28 μA/m^2	-	-
Case 3	3.12 μA/m^2	3.12 μA m^{-2}	8 × 10^{-5} μA m^{-2}
Case 4	3.12 μA/m^2	3.12 μA m^{-2}	5 × 10^{-5} μA m^{-2}
Case 5	3.10 μA/m^2	3.10 μA m^{-2}	5 × 10^{-5} μA m^{-2}
Case 6	6.94 μA/m^2	4.42 μA m^{-2}	2.52 μA m^{-2}
Case 7	32.54 μA/m^2	4.30 μA m^{-2}	28.24 μA m^{-2}

[30] The current densities of each of seven solutions are summarized in Table 3. From these results, it is clear that the current density increases with increasing torus H^+ density; however, the primary current density carrier is the electron. Although Io H^+ ions make no contribution below the potential drop due to the reflection by the large potential barrier, they play an important role in assisting precipitating electrons to reach a higher density and a higher current density for the solution.

3.6. Auroral Cavity

[31] As demonstrated earlier, two potential jumps are formed at 1.5 and 2.2 R_J, respectively (see cases 5–7) if a high secondary electron density is imposed. These two potential drops separate the spatial domain into three regions where the low-latitude region is dominated by ionosphere plasma and the high-latitude region is dominated by Io plasma. The region between these layers is dominated by energized ionospheric ions and energized electrons. There is little or no cold plasma in the region between the two potential drops, and hence this region is called an auroral cavity or density cavity.

[32] Figure 8 shows a phase-space distribution function of hot electrons inside the auroral cavity at 1.86 R_J in Figure 6. The horizontal axis represents the velocity parallel to the magnetic field with the positive direction toward Jupiter's ionosphere, while the vertical axis represents the perpendicular velocity. A loss cone can be seen in the negative V_{para} direction (toward Io). The electron cyclotron maser instability has been used to explain auroral radio

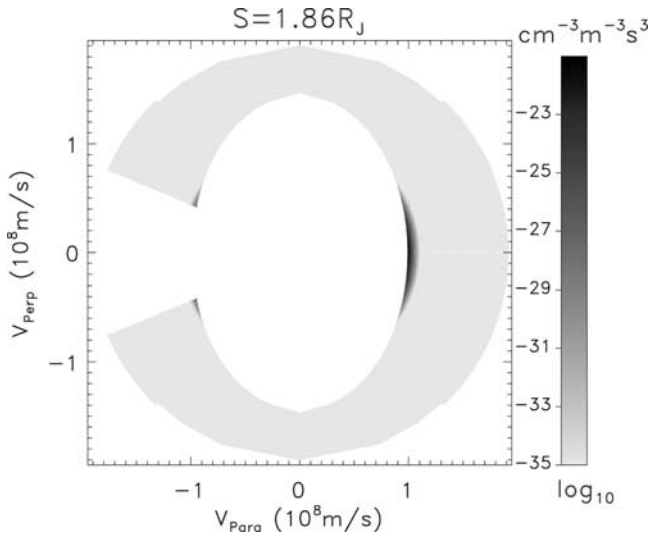

Figure 8. Electron phase-space density distribution in the aurora cavity from case 6.

emissions [*Zarka*, 1998, and references therein]. On the basis of particle and field observations by the FAST satellite in the Earth's polar orbit, *Ergun et al.* [2000b] indicated that AKR results from an unstable horseshoe or shell electron distribution and concluded that the shell electron cyclotron maser was the source mechanism of AKR. Their findings also suggest parallel electric fields as a fundamental particle acceleration mechanism in planetary radiation [*Ergun et al.*, 2001b]. In Figure 8 a horseshoe electron distribution can be seen inside the auroral cavity due to the large parallel electric field. This unstable distribution is a candidate for the trigger that induces the shell electron cyclotron maser instability and generates the Io-controlled DAM.

[33] The electron energy of 30 keV calculated by *Gérard et al.* [2002] at the tail emission was based on the electron precipitation and Jovian atmosphere models. This calculated value may vary with different models. Moreover, the electron energy decreases with increasing distance relative to Io's footprint. A 10 kV potential was also selected as the boundary condition for comparison (results not shown). The location of the auroral cavity is similar to its position when applying a 30 kV boundary condition. The total precipitating electron energy flux from the solution with the 30 kV potential is 3 times higher than with a 10 kV potential. On the other hand, a 10 kV potential requires a current density a factor 3 times higher than a 30 kV potential in order to maintain the same energy flux. From this, it can be concluded that although the potentials or current densities may vary, the fundamental characteristics of the auroral cavities are similar.

4. Discussions and Conclusions

[34] In this paper, studies of parallel electric fields are presented based on a large-scale static Vlasov model along the magnetic field line applicable to the static upward current region of Io's wake. The following predictions and suggestions can be drawn from our solutions:

1. Vlasov modeling of the magnetic flux tube in the upward current region of Io's wake demonstrates that self-consistent solutions with 30 keV potential drops are viable and consistent with the observed emissions in Jupiter's ionosphere at the magnetic footprint downstream of Io and with the known constraints on the plasma conditions in Jupiter's ionosphere and the Io torus. The large acceleration potentials form near the minimum of the combination of gravitational and centrifugal potentials where the ionospheric plasma density is comparable to Io plasma density. The width of the potential jump is narrower than the resolution of the spatial grid size (roughly 0.16 R_J).

2. The numerical solutions (cases 1–3) show that an enhanced density of hot electrons in the Io torus can dramatically increase the electron energy flux into Jupiter's ionosphere. The result of case 3 suggests that the current density tends to be carried by hot electrons. We suggest that the determination of hot electrons in the Io torus should be a high priority in future studies.

3. A sufficiently high secondary electron density causes an auroral cavity to be formed between two transition layers at $\sim$1.5–2.2 R_J Jovicentric distance along the magnetic field line. The lower transition layer appears at an altitude where the secondary electron density is equal to the cold ionospheric proton density. If this condition is not met, only a single potential drop is formed (as seen in case 4). Stronger precipitating electron flux (and hence higher secondary electron density) causes a second potential drop to appear at a lower altitude.

4. The current density in the flux tube is extremely sensitive to the density of light ions in Io's torus. Although iogenic H^+ ions make no contribution inside the auroral cavity due to their reflection by the large potential barrier, they play an important role in assisting precipitating electrons reach higher density levels and attain a higher current density in the solution. It should be noted that the current density is always carried by electrons. On the basis of our solutions, the current density of the flux tube increases with increasing torus H^+ density. Measurement of H^+ density at high latitudes is critical for understanding torus-ionosphere coupling. The numerical solutions show that heavy ions are tightly confined near the torus by the centrifugal potential. On the other hand, the ambipolar electric field exceeds the centrifugal potential for H^+ ions, so the H^+ ions are actively expelled from the torus rather than confined. The results of our model indicate the proton density in the Io wake flux tubes to be less than $\sim$1 cm^{-3} in order to obtain a precipitating energy flux of the order of the magnitude (a few ergs cm^{-2} s^{-1}) estimated from the auroral emissions observed downstream of Io's footprint by STIS/HST [*Clarke et al.*, 2002; *Gérard et al.*, 2002]. When comparing the proton densities derived from our model with observations, it must be kept in mind that the plasma in the flux tubes downstream of Io may not be typical of the neighboring torus. Nevertheless, we point out that (1) if protons comprise >0.5% of the torus ions (density > 6 cm^{-3}), then the current density would be 3 orders of magnitude higher than recent calculations from observations; (2) the brightness values reported by *Clarke et al.* [2002] are based on an assumed 0.014 counts s^{-1} kR^{-1} per 0.08 arcsec resolution, which smears out fine structures of auroral arcs. Additionally, the estimated current density and precipitating electron energy are based on model calculations that may vary with different selected models; (3) there may be fine auroral arcs with spatial sizes smaller than the instrument resolution. These fine structures may be a result of the higher current density and energy flux in the flux tube, but may not be observable due to the limited instrument resolution.

5. A horseshoe or shell electron distribution is obtained inside the auroral cavity due to a large parallel electric field. This unstable distribution may trigger the shell cyclotron maser instability [*Ergun et al.*, 2000b] and provide the necessary free energy for the growth of radio emissions. Thus our model predicts that the flux tubes downstream from Io should contribute to the Io-controlled decameter (DAM) radiation [e.g., *Leblanc et al.*, 1994; *Queinnec and Zarka*, 1998]. The model predicts that the auroral cavity is located from $\sim$1.5 to 2.2 R_J at about 20° downstream from Io, so this particular downstream contribution is confined to the frequency range of $\sim$3 to $\sim$12 MHz. Our result is consistent with that shown in Figure 7.1 of *Dessler* [1983], where the peak in the DAM is centered on $\sim$10 MHz extending over a band approximately 4 MHz wide. The modeling predicts that

the higher-frequency (~20–25 MHz) Io-controlled DAM should come from a location nearer to Jupiter's ionosphere since the lower ionospheric scale height will force the cavity to lower altitudes. A more detailed investigation into the implications of the model on Io-controlled DAM is the subject of a future study.

[35] We must caution the reader of this study to be aware that results are determined from the boundary conditions and that solutions may not be unique; however, the large-scale results provide a basis to investigate time-independent, self-consistent parallel electric fields and seek for confirmation from future in situ field and particle measurements.

[36] **Acknowledgments.** The authors wish to thank John Clarke, Jean-Claude Gérard, Wayne Pryor, Joe Ajello, Frank Crary, Philippe Zarka, Bill (W. K.) Peterson, and Laila Andersson for helpful information and useful conversations. The work was supported by NASA grants NAG5-7088 and JPL 959550 to the University of Colorado.

[37] Arthur Richmond thanks the reviewers for their assistance in evaluating this paper.

References

Ajello, J. M., D. E. Shemansky, W. R. Pryor, A. I. Stewart, K. E. Simmons, T. Majeed, J. H. Waite, G. R. Gladstone, and D. Crodent, Spectroscopic evidence for high-altitude aurora at Jupiter from Galileo extreme ultraviolet spectrometer and Hopkins ultraviolet telescope observations, *Icarus*, *152*, 151, 2001.

Andersson, L., R. E. Ergun, D. Newman, J. P. McFadden, C. W. Carlson, and Y.-J. Su, Characteristics of parallel electric fields in the downward current region of the aurora, *Phys. Plasmas*, *9*, 3600, 2002.

Bagenal, F., Empirical model of the Io plasma torus: Voyager measurements, *J. Geophys. Res.*, *99*, 11,043, 1994.

Bigg, E. K., Influence of the satellite Io on Jupiter's decametric emission, *Nature*, *203*, 1008, 1964.

Carlson, C. W., et al., FAST observations in the downward auroral current region: Energetic upgoing electron beams, parallel potential drops, and ion heating, *Geophys. Res. Lett.*, *25*, 2017, 1998.

Chaston, C. C., C. W. Carlson, W. J. Peria, R. E. Ergun, and J. P. McFadden, FAST observations of inertial Alfvén waves in the dayside aurora, *Geophys. Res. Lett.*, *26*, 647, 1999.

Chust, T., A. Roux, S. Perraut, P. Louarn, W. S. Kurth, and D. A. Gurnett, Galileo plasma wave observations of iogenic hydrogen, *Planet. Space Sci.*, *47*, 1377, 1999.

Clarke, J. T., et al., Far-ultraviolet imaging of Jupiter's aurora and the Io "footprint", *Science*, *274*, 404, 1996.

Clarke, J. T., et al., Ultraviolet emissions from the magnetic footprints of Io, Ganymede and Europa on Jupiter, *Nature*, *415*, 997, 2002.

Crary, F. J., On the generation of an electron beam by Io, *J. Geophys. Res.*, *102*, 37, 1997.

Crary, F. J., F. Bagenal, J. A. Ansher, D. A. Gurnett, and W. S. Kurth, Anisotropy and proton density in the Io plasma torus, *J. Geophys. Res.*, *101*, 2699, 1996.

Crary, F. J., F. Bagenal, L. A. Frank, and W. R. Paterson, Galileo plasma spectrometer measurements of composition and temperature in the Io plasma torus, *J. Geophys. Res.*, *103*, 29,359, 1998.

Delamere, P. A., F. Bagenal, R. E. Ergun, and Y.-J. Su, Momentum transfer between the Io plasma wake and Jupiter's ionosphere, *J. Geophys. Res.*, *108*, doi:10.1029/2002JA009530, in press, 2003.

Dessler, A. J., *Physics of the Jovian Magnetosphere*, Cambridge Univ. Press, New York, 1983.

Dols, V., J. C. Gérard, J. T. Clarke, J. Gustin, and D. Grodent, Diagnostics of the Jovian aurora deduced from ultraviolet spectroscopy: Model and HST/GHRS observations, *Icarus*, *147*, 251, 2000.

Ergun, R. E., et al., FAST satellite observations of large-amplitude solitary structures, *Geophys. Res. Lett.*, *25*, 2041, 1998.

Ergun, R. E., C. W. Carlson, J. P. McFadden, F. S. Mozer, and R. J. Strangeway, Parallel electric fields in discrete arcs, *Geophys. Res. Lett.*, *27*, 4053, 2000a.

Ergun, R. E., C. W. Carlson, J. P. McFadden, G. T. Delory, R. J. Strangeway, and P. L. Pritchett, Electron-cyclotron maser driven by charged-particle acceleration from magnetic field-aligned electric fields, *Astrophys. J.*, *538*, 456, 2000b.

Ergun, R. E., Y.-J. Su, L. Andersson, C. W. Carlson, J. P. McFadden, F. S. Mozer, D. L. Newman, M. V. Goldman, and R. J. Strangeway, Direct observation of localized parallel electric fields in a space plasma, *Phys. Rev. Lett.*, *87*, 45,003, 2001a.

Ergun, R. E., Y.-J. Su, and F. Bagenal, Terrestrial radio emission: AKR, in *Planetary Radio Emissions V*, edited by H. O. Rucker, M. L. Kaiser, and Y. Leblanc, p. 271, Osterreichischen Akad. der Wiss., Vienna, Austria, 2001b.

Ergun, R. E., L. Andersson, D. S. Main, Y.-J. Su, C. W. Carlson, J. P. McFadden, F. S. Mozer, and R. J. Strangeway, Parallel electric fields in the upward current region of the aurora: Indirect and direct observations, *Phys. Plasmas*, *9*, 3685, 2002a.

Ergun, R. E., Y.-J. Su, F. Bagenal, and P. A. Delamere, Recent M-I coupling discoveries and how they apply to the outer planets, Magnetospheres of Outer Planets meeting, July 2002b.

Frank, L. A., and W. R. Paterson, Intense electron beams observed at Io with the Galileo spacecraft, *J. Geophys. Res.*, *104*, 28,657, 1999a.

Frank, L. A., and W. R. Paterson, Production of hydrogen ions at Io, *J. Geophys. Res.*, *104*, 10,345, 1999b.

Frank, L. A., and W. R. Paterson, Observations of plasmas in the Io torus with the Galileo spacecraft, *J. Geophys. Res.*, *105*, 16,017, 2000.

Gérard, J.-C., and V. Singh, A model of energetic electrons and EUV emission in the Jovian and Saturnian atmospheres and implications, *J. Geophys. Res.*, *87*, 4525, 1982.

Gérard, J.-C., J. Gustin, D. Grodent, P. Delamere, and J. T. Clarke, The excitation of the FUV Io tail on Jupiter: Characterization of the electron precipitation, *J. Geophys. Res.*, *107*(A11), 1394, doi:10.1029/2002JA009410, 2002.

Goldreich, P., and D. Lynden-Bell, Io, a Jovian unipolar inductor, *Astrophys. J.*, *156*, 59, 1969.

Grodent, D., J. H. Waite Jr., and J. C. Gérard, A self-consistent model of the Jovian auroral thermal structure, *J. Geophys. Res.*, *106*, 12,933, 2001.

Hill, T. W., and V. M. Vasyliunas, Jovian auroral signature of Io's corotational wake, *J. Geophys. Res.*, *107*(A12), 1464, doi:10.1029/2002JA009514, 2002.

Knight, S., Parallel electric fields, *Planet. Space Sci.*, *21*, 741, 1973.

Lebanc, Y., G. A. Dulk, and F. Bagenal, On Io's excitation and the origin of Jupiter's decametric radiation, *Astron. Astrophys.*, *290*, 660, 1994.

Le Quéau, D., R. Pellat, and A. Roux, Theory of planetary radio emissions, *Adv. Space Res.*, *3*, 25, 1983.

Lotko, W., A. V. Streltsov, and C. W. Carlson, Collisionless resistivity, particle acceleration, auroral arcs in a simulated and an observed shear Alfvén resonance, *Eos Trans. AGU*, *79*(17), Spring Meet. Suppl., S310, 1998.

Lyons, L. R., Generation of large-scale regions of auroral currents, electric potentials, and precipitation by the divergence of the convection electric field, *J. Geophys. Res.*, *85*, 17, 1980.

Lysak, R. L., The relationship between electrostatic shocks and kinetic Alfvén waves, *Geophys. Res. Lett.*, *25*, 2089, 1998.

Mauk, B. H., D. J. Williams, and Aharon Eviatar, Understanding Io's space environment interaction: Recent energetic electron measurements from Galileo, *J. Geophys. Res.*, *106*, 26,195, 2001.

Mauk, B. H., B. J. Anderson, and R. M. Thorne, Magnetosphere-ionosphere coupling at Earth, Jupiter, and beyond, in *Atmospheres in the Solar System: Comparative Aeronomy*, *Geophys. Monogr. Ser.*, vol. 130, edited by M. Mendillo, A. Nagy, and J. H. Waite, pp. 97–114, AGU, Washington, D. C., 2002.

Melrose, D. B., and G. A. Dulk, On the elliptical polarization of Jupiter's decametric radio emission, *Astron. Astrophys.*, *249*, 250, 1991.

Mozer, F. S., and C. A. Kletzing, Direct observation of large, quasi-static, parallel electric fields in the auroral acceleration region, *Geophys. Res. Lett.*, *25*, 1629, 1998.

Neubauer, F. M., Nonlinear standing Alfvén wave current system at Io: Theory, *J. Geophys. Res.*, *85*, 1171, 1980.

Prangé, R., D. Rego, D. Southwood, P. Zarka, S. Miller, and W. Ip, Rapid energy dissipation and variability of the Io-Jupiter electrodynamic circuit, *Nature*, *379*, 323, 1996.

Queinnec, J., and P. Zarka, Io-controlled decameter arcs and Io-Jupiter interaction, *J. Geophys. Res.*, *103*, 26,649, 1998.

Sittler, E. C., Jr., and D. F. Strobel, Io plasma torus electrons: Voyager 1, *J. Geophys. Res.*, *92*, 5741, 1987.

Tokar, R. L., D. A. Gurnett, F. Bagenal, and R. R. Shaw, Light ion concentrations in Jupiter's inner magnetosphere, *J. Geophys. Res.*, *87*, 2241, 1982.

Waite, J. H., Jr., T. E. Cravens, J. U. Kozyra, A. F. Nagy, S. K. Atreya, and R. H. Chen, Electron precipitation and related aeronomy of the Jovian thermosphere and ionosphere, *J. Geophys. Res.*, *88*, 6143, 1983.

Wang, K., R. M. Thorne, R. B. Horne, and W. S. Kurth, Constraints on Jovian plasma properties from a dispersion analysis of unducted whistlers in the warm Io torus, *J. Geophys. Res.*, *103*, 14,979, 1998a.

Wang, K., R. M. Thorne, R. B. Horne, and W. S. Kurth, Cold torus whistlers: An indirect probe of the inner Jovian plasmasphere, *J. Geophys. Res.*, *103*, 14,987, 1998b.

Zarka, P., Auroral radio emissions at the outer planets: Observations and theories, *J. Geophys. Res.*, *103*, 20,159, 1998.

Zarka, P., J. Queinnec, and F. J. Crary, Low-frequency limit of Jovian radio emissions and implications on source locations and Io plasma wake, *Planet. Space Sci.*, *49*, 1137, 2001.

F. Bagenal, P. A. Delamere, R. E. Ergun, and Y.-J. Su, Laboratory for Atmospheric and Space Physics, University of Colorado, 1234 Innovation Drive, Boulder, CO 80303, USA. (bagenal@colorado.edu; delamere@lasp.colorado.edu; ree@fast.colorado.edu; ysu@lasp.colorado.edu)

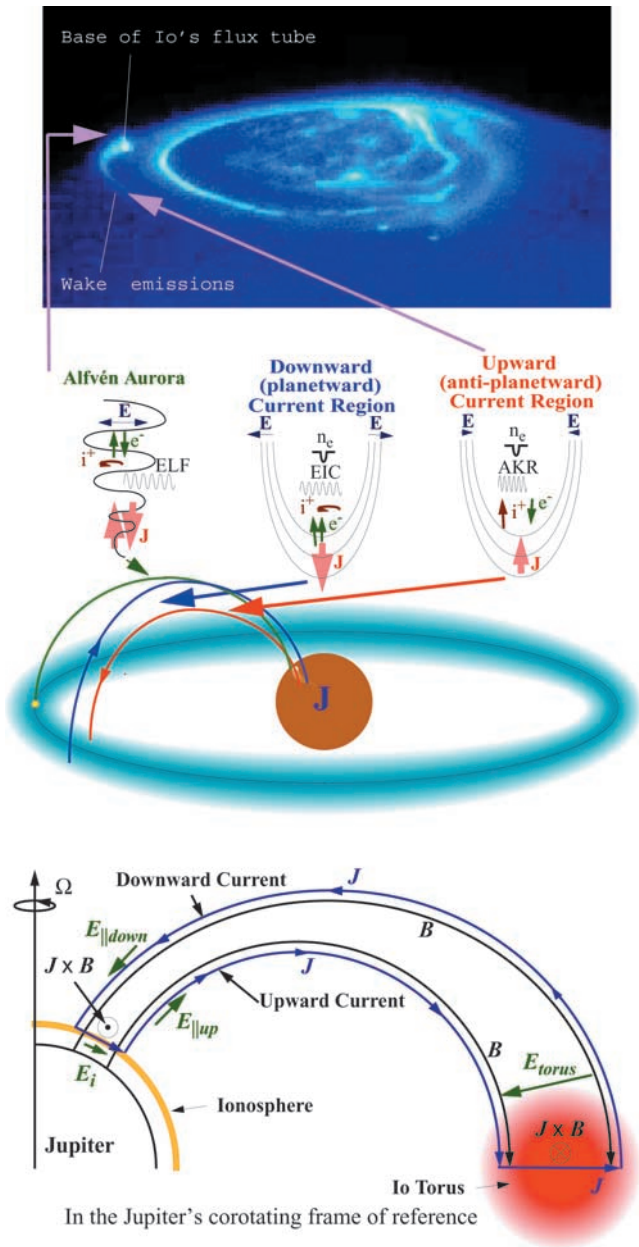

Figure 1. The top panel shows a Jovian auroral image taken by the Hubble Space Telescope [after *Clarke et al.*, 2002, Figure 1b], where the Io-induced aurora is seen on the left with the brightest emissions at the base of the Io flux tube and an emission trail extending downstream. A depiction of the three types of Jovian auroral regions is shown in the middle panel, where the green, blue, and red lines represent the Alfvén-dominated region, the downward current region, and the upward current region, respectively. The quasi-static current structure downstream of Io's wake in the Jupiter's corotating frame of reference is illustrated in the bottom panel, where black and blue lines are used to represent the magnetic field and electric current, respectively. Green arrows are used to show the electric field, where $E_{\text{torus}} = E_i + E_{\|\text{up}} + E_{\|\text{down}}$.